Surface Flow Patterns and Aerodynamic Heating on Space Shuttle Vehicles

J. G. MARVIN,* H. L. SEEGMILLER,† W. K. LOCKMAN,† G. G. MATEER,‡
C. C. PAPPAS,‡ AND C. E DEROSE‡
NASA Ames Research Center, Moffett Field, Calif.

Surface oil flow photographs, pressure distributions, and heating distributions on models of typical vehicles are presented and analyzed. The test data, obtained at $M_\infty = 7.4$ for Reynolds numbers between 1 and 10 million and for angles of attack to 60°, include laminar, transitional, and turbulent heating data on straight-wing and delta-wing vehicles. Boundary-layer transition, including effects of simulated joints between heat-shield panels, and some unusual heating patterns on smooth models are described.

Nomenclature

C = width of body
D = diameter of reference sphere
H = total enthalpy
h = metric coefficient defined by Eq. (4)
L = model axial length from nose
M = Mach number
p = pressure
$\dot{q}$ = heating rate
R = radius of reference sphere
r = Chine radius
$\bar{r}$ = radius of curvature of the body lower surface in the cross section plane
Re = Reynolds number
s = surface length in cross flow direction
T = temperature
u, v = cross flow and axial velocity
x = axial length from nose
$\bar{x}$ = distance along windward streamline
α = angle of attack
δ_E = elevon deflection angle
ε = emissivity

Subscripts

aw = adiabatic wall
CYL = cylinder
e = edge of boundary layer
eq = equivalent length
l = local value
L = based on model axial length
o = total stagnation value
s = sphere
sL = stagnation line
t = at transition
t_2 = total value behind normal shock
w = wall
θ = momentum thickness
∞ = freestream

Introduction

THE space shuttle transportation system is a fully reusable two-stage system with boost and orbiting stages capable of returning to the launch site and making wheeled landings.[1] The system's success depends on the integration of solutions to problems involving many disciplines, one of which is entry aerothermodynamics. To evaluate the system properly requires the definition of the thermal environment for a wide range of Mach numbers, Reynolds numbers, and angles of attack.

NASA has taken an active role in providing a broad data base for evaluating the aerothermodynamic technology requirements and the vehicle concepts being studied by industry contractors. Studies on aerodynamic heating problems have been reported in Refs. 2 and 3 and other documents with limited distribution (see reference section of Ref. 2). This paper will focus attention on the recent results and illustrate by example the progress made in evaluating aerothermodynamic technology as applied to the space shuttle.

Theory

Laminar heat-transfer data obtained on the centerline of the windward surface at high angle of attack are later compared with predictions using a modification of infinite swept cylinder theory.[4] A ratio of heat-transfer rates along the symmetry or stagnation line of the windward surface at any axial location can be formed as follows:

$$\frac{\dot{q}_{sL}}{\dot{q}_s} = \left[\frac{\dot{q}_{\mathrm{CYL},\alpha_l=90^\circ}}{\dot{q}_s}\right]\left[\frac{\dot{q}_{\mathrm{CYL},\alpha_l}}{\dot{q}_{\mathrm{CYL},\alpha_l=90^\circ}}\right]\left[\frac{\dot{q}_{sL}}{\dot{q}_{\mathrm{CYL},\alpha_l}}\right] \tag{1}$$

Substituting expressions from Ref. 4 for the first and third bracketed terms and from Ref. 5 for the second term results in

$$\frac{\dot{q}_{sL}}{\dot{q}_s} = 0.714\left(\frac{D}{C}\right)^{1/2}\left[\left(\sin^{1.1}\alpha_l\right)\frac{H_{aw}-H_w}{H_o-H_w}\right]\left[\frac{(du_e/ds)_{sL}}{(du_e/ds)_{\mathrm{CYL},\alpha_l}}\right]^{1/2} \tag{2}$$

The last bracketed term, the ratio of velocity gradients for the actual body compared to a cylinder of the same dimension, can be calculated analytically by the method described in Ref. 6 or given by the correlation taken from Ref. 7 that is limited to high Mach number and ideal gas

$$\frac{(du_e/ds)_{sL}}{(du_e/ds)_{\mathrm{CYL},\alpha_l}} = \frac{0.745 + 3.14(r/C)}{2.315} \tag{3}$$

Laminar and turbulent heating rates along the windward centerline are also compared later with theory modified to account for streamline divergence. The expression used to obtain the divergence on the windward line[8] was

$$(1/h)(\partial h/\partial \bar{x}) = (1/\bar{r})(\partial \bar{r}/\partial \bar{x}) + (1/v_e)(\partial u_e/\partial s) \tag{4}$$

where the velocity gradient was evaluated from Eq. (3) using the Newtonian value for $(du_e/ds)_{\mathrm{CYL}}$. For flat-plate or strip

Presented as Paper 71-594 at the AIAA 4th Fluid and Plasma Dynamics Conference, Palo Alto, Calif., June 21–23, 1971; submitted June 28, 1971; revision received March 27, 1972.

Index categories: Entry Vehicles and Landers; Boundary Layers and Convective Heat Transfer—Laminar; Boundary Layers and Convective Heat Transfer—Turbulent.

* Chief, Experimental Fluid Dynamics Branch, Thermo- and Gas-Dynamics Division. Associate Fellow AIAA.
† Research Scientist. Member AIAA.
‡ Research Scientist.

theory applications the modification was accomplished by replacing the distance from the leading edge or flow origin by an equivalent length given for laminar flow by[8]

$$x_{eq} = (\int^{x} h^2\, dx)/h^2 \tag{5}$$

and for turbulent flow by[9]

$$x_{eq} = (\int^{x} h\, dx)/h \tag{6}$$

For applications employing a nonsimilar laminar boundary-layer computer program[10] the modification was accomplished by solving the axisymmetric analog form of the boundary-layer equations[11] which replace the usual axisymmetric radius generator with the metric coefficient h.

Facility and Test Conditions

The test data were obtained in the Ames 3.5 ft Hypersonic Wind Tunnel.[12,13] A test cabin equipped with a model insert mechanism was attached to the test section. Sliding doors, matched to the inside contour of the test section, shielded the models inside the cabin from the main flow while steady flow was established. Models inserted into the stream usually reached the tunnel centerline in less than 0.5 sec.

The data were taken at a Mach number of 7.4 for a range of freestream Reynolds numbers, based on model length, between 1 and 10 million. Angle of attack was varied between 15° and 60°. The nominal freestream total temperature varied between 778°K (1400°R) and 833°K (1500°R). Nominal model wall temperatures were 300°K (540°R) for the thermocouple tests and 340°K (610°R) for the paint and oil flow tests.

Configurations

The configurations studied represent typical space shuttle orbiter concepts. The Manned Spacecraft Center (MSC) straight wing was proposed by Faget for a 200-naut miles crossrange mission.[14] The remaining configurations are 200-naut miles and 1100 naut miles crossrange vehicles developed by North American Rockwell (NAR). Two delta-wing configurations were studied. Both had geometrically similar fuselages but the 129 configuration had a slightly larger wing area and a thicker fuselage profile above the wing.

The test data were obtained on scaled models of these configurations. Most of the heating data were obtained by measuring the transient temperature response of thin-walled models instrumented with thermocouples but, as mentioned later, some delta-wing data were obtained using the phase change paint technique[15] on a model constructed from stycast. These latter data as well as the oil flow photographs on the delta wing are the only data presented for models of the 129 configuration. The photographs of the oil flow patterns were taken after the models were retracted from the stream.

Results and Discussion

Windward surface data on the straight-wing configuration are presented first. Only data at high angle of attack, $\alpha = 60°$, are of interest because this configuration flies a maximum-lift maximum-drag trajectory to minimize the total heat input. Results on the delta wing are presented next. Data for a range of angles-of-attack are of interest for this configuration, because it flies a variable lift-to-drag trajectory to obtain crossrange using angle-of-attack and bank-angle modulation to minimize heating rate and total heat input. Boundary-layer transition from laminar to turbulent flow for both vehicles is considered at the end of this section.

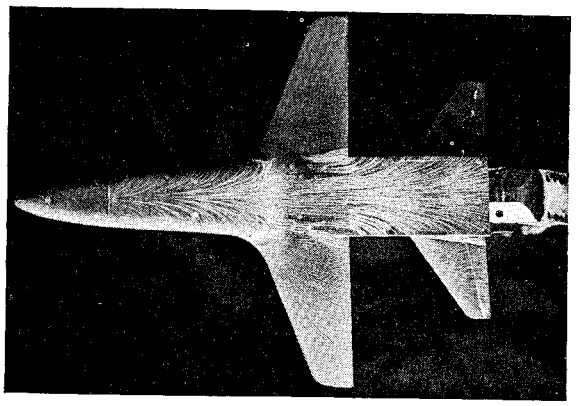

Fig. 1 Windward surface oil-flow photograph of NAR straight-wing orbiter; $Re_{\infty_L} = 1.4 \times 10^6$ and $\alpha = 60°$.

Straight Wing Orbiters

Figure 1 is a photograph of an oil flow pattern representing the surface streamline directions on the lower surface of the NAR straight-wing orbiter at $\alpha = 60°$. Patterns showing significant crossflow are formed on the fuselage ahead and downstream of the wing. The influence of the wing on the fuselage pattern appears as an oil buildup and a rapid turning of the streamlines near the wing fillet resulting from the increase in fuselage pressure due to the presence of the wing. On the wing itself, a stagnation region appears with a reversed flow near the fillet and a stagnation line emanates from the region. This photograph is helpful in interpreting the pressure and heating distributions presented next.

Normalized pressures and heating rates on the windward surface centerline are plotted vs axial distance along the fuselage in Fig. 2. The bar on the heating data points indicates the heating variation across the fuselage. The pressures, normalized by the normal shock pressure, decrease with distance from the stagnation region, rise sharply in the wing region, and then decrease. No significant measurable differences in pressure distribution occurred for the range of Reynolds number in Fig. 2. Over most of the fuselage the

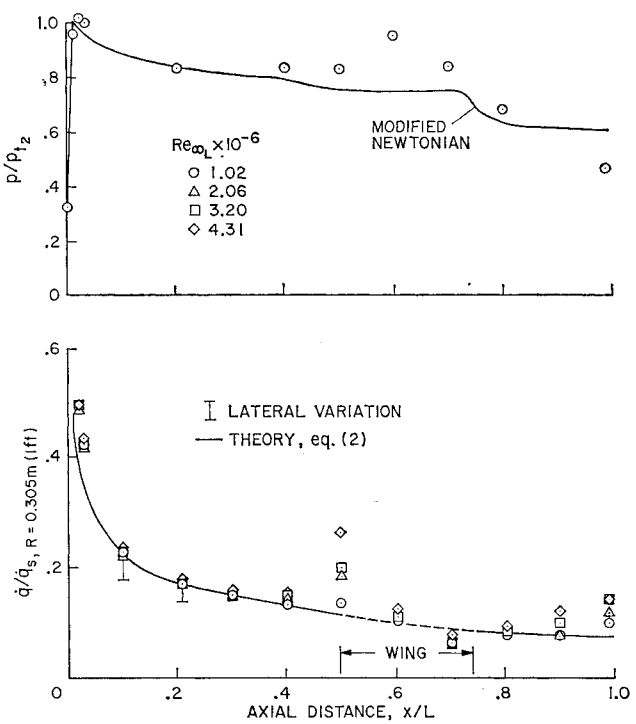

Fig. 2 Centerline pressures and heating rates on NAR straight-wing orbiter; 0.006 scale, $L = 0.315$ m, and $\alpha = 60°$.

measured pressures are somewhat higher than the modified Newtonian prediction. A clear exception occurs at the most rearward station where the measured pressure is probably affected by the expansion of the flow around the model base.

The heating rates were normalized by a theoretical sphere heating rate[16] evaluated for the wind-tunnel test conditions and with a radius equivalent to 0.305 m (1 ft) on the full-scale vehicle. The lowest test Reynolds number corresponds to the value for the full-scale vehicle near peak heating. At the beginning of the wing region, the normalized rates increase with increasing Reynolds number, indicating the complex nature of the flow in this region. The data toward the rear of the fuselage also depend on Reynolds number, indicating that transition to turbulent flow may have taken place. The laminar theory line represents the rates predicted using modified swept-cylinder theory [i.e., Eqs. (2) and (3)]. Beyond $x/L = 0.1$, the theory and data agree well, except where Reynolds number effects occurred. Similar comparisons for $\alpha = 30°$ and 15° and for $\alpha = 60°$ at $M_\infty = 15$[2] indicate that modified swept cylinder theory will provide adequate estimates of the windward laminar heating rates. As shown in Ref. 2 the lateral variation in heating can be estimated by the cross flow theory from Ref. 4.

Wing pressures and heating rates for one Reynolds number are shown in Fig. 3. At a given span location the pressures increase rapidly from the leading edge to the 10% chord location and decrease slightly thereafter. Inboard of the 20% semispan location the pressures near the stagnation region on the fillet exceed the normal shock pressure. Except for the wing leading edge, the majority of the measured pressures have essentially the same magnitude as on the fuselage centerline at $x/L = 0.6$ where the pressure showed an abrupt increase.

The heating data illustrate a serious problem encountered by the straight-wing vehicles. The heating is high in the vicinity of the leading edge, peaking near the 25% semispan location where the effect of the body and wing shock interference is maximum.[17] However, the higher heating region is confined to the forward 25% of the chord which represents only a small area of the wing that could be ablatively protected. Although the data are not presented, tests performed over a Reynolds number range between 1 and 4 million indicated increased heating on the wing with increased Reynolds number.

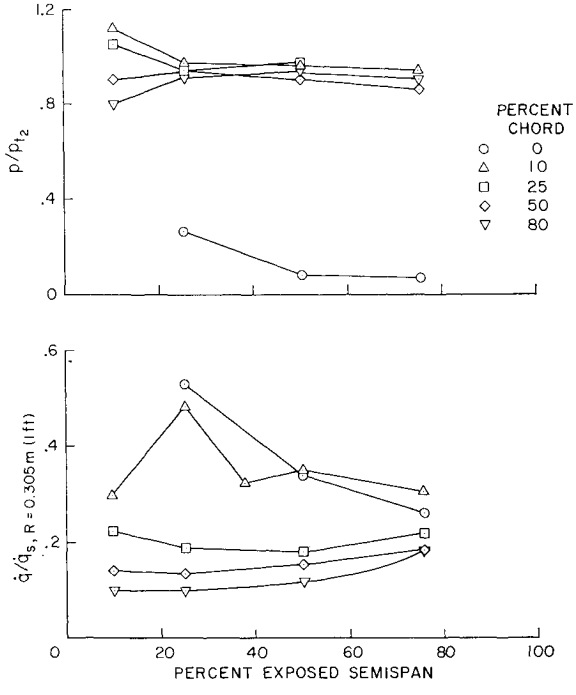

Fig. 3 Wing pressures and heating rates on NAR straight-wing orbiter; $Re_{\infty L} = 1.02 \times 10^6$, $L = 0.315$ m, and $\alpha = 60°$.

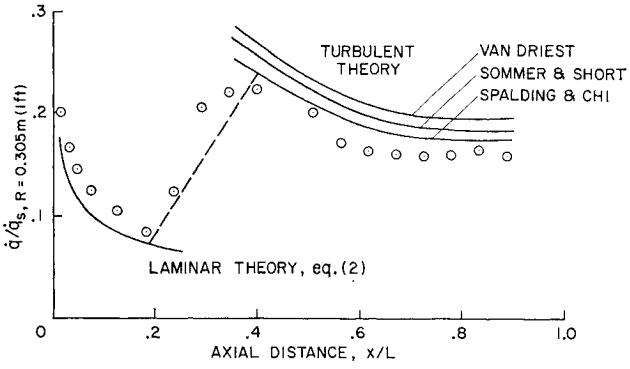

Fig. 4 Centerline turbulent heating rates on MSC straight-wing orbiter fuselage; 0.01 scale, $Re_{\infty L} = 9.6 \times 10^6$, $L = 0.466$ m, and $\alpha = 40°$.

Heating tests at high Reynolds numbers on the fuselage of an MSC orbiter model without the wing were made to obtain boundary-layer transition and turbulent heating data. Typical results are shown in Fig. 4. The data show typical laminar heating away from the stagnation point, a region of transitional heating, followed by turbulent heating. The data are compared with a laminar theory and the three turbulent strip theories discussed in Ref. 18. The theories are connected with a linear curve in the transition region where the Reynolds number at the end of transition was assumed to be twice the Reynolds number at the measured onset of transition. The modified swept cylinder theory given by Eq. (2) predicts the heating rates reasonably well. Each turbulent theory was modified to account for flow divergence using Eq. (6) but the corrections were small. The boundary-layer edge conditions were taken to be those for a swept cylinder; the origin of turbulent flow was assumed located at the beginning of transition; and the Reynolds analogy factor was assumed to be 1.0, a value experimentally verified by data on plates and cones tested in the same facility.[18] The turbulent level is predicted somewhat better by the Spalding and Chi theory. It should be noted that turbulent predictions based on boundary-layer-edge conditions obtained by isentropic expansion from normal shock to the local Newtonian pressure underpredicted the data.

Delta Wing Orbiters

Photographs of the surface oil flow patterns on a delta-wing vehicle for various angles of attack were taken to assess qualitatively the complexity of the flowfield. An example of the patterns formed on the windward side of the 129-delta wing at $\alpha = 15°$ is shown in Fig. 5. Over the fuselage ahead of the wing the patterns are not unlike the patterns formed on the straight wing orbiter model shown previously. Over the wing the flow is more complex. For this test, elevons were deflected into the flow and separation and reattachment regions are visible. Near the centerline, surface streamlines flow straight back whereas away from the centerline the swept leading edge causes the flow to turn in. This pattern of inward flow from

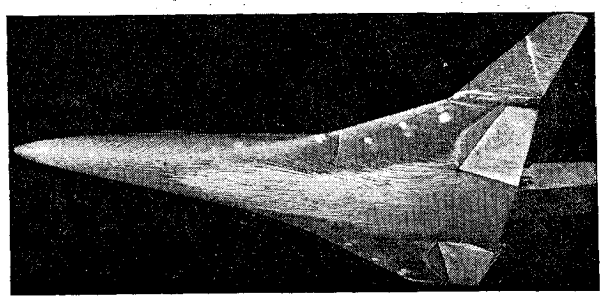

Fig. 5 Windward surface oil-flow photograph of NAR-129 delta-wing orbiter; 0.008 scale, $Re_{\infty L} = 1.4 \times 10^6$, and $\alpha = 15°$.

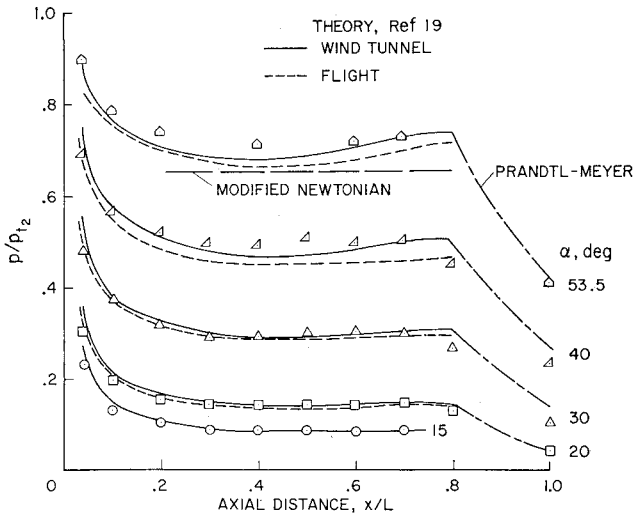

Fig. 6a Windward centerline pressures and heating on NAR 134 delta-wing orbiter; 0.006 scale, $Re_{\infty L} = 1.0 \times 10^6 - 4 \times 10^6$, and $L = 0.323$ m; pressures.

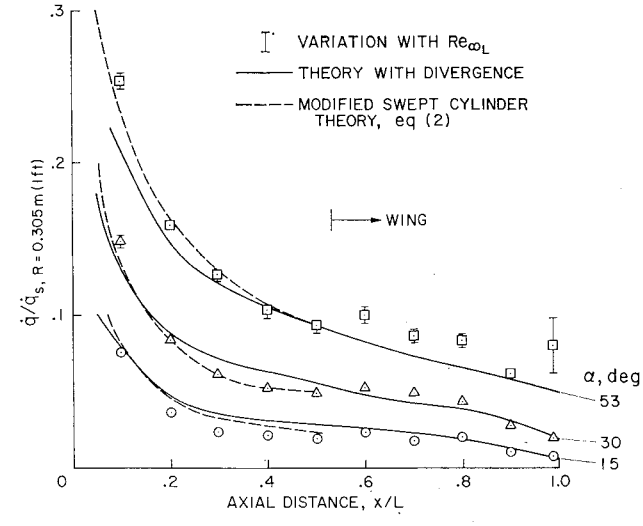

Fig. 6b Windward centerline pressures and heating on NAR 134 delta-wing orbiter; 0.006 scale, $Re_{\infty L} = 1.0 \times 10^6$, and $L = 0.323$ m; heating.

the leading edge changes with angle-of-attack. For example, at $\alpha = 50°$ a stagnation line is visible downstream of the wing leading edge and the surface streamline direction aft of this line is nearly parallel with the leading edge.

Windward centerline pressures and heating on the delta wing for various angles of attack are plotted vs axial distance in Fig. 6. At each angle of attack the pressures decrease with distance from the stagnation region, remain relatively constant over the flat portion of the body, and then decrease rapidly beyond $x/L = 0.8$ where boattailing of the body surface occurs. The solid line represents a prediction by Kaattari of Ames that applies an equivalent-elliptic-cone-method locally.[19] Good agreement between theory and experiment is obtained at all angles of attack. Over the boattailed section, Prandtl-Meyer theory predicts the decrease in pressure. Also shown at the highest angle of attack is a modified Newtonian prediction of the pressure over the flat portion of the body surface. For this and all other angles of attack, modified Newtonian theory underpredicts the pressures by 15–20%. As shown by the dashed line, an extrapolation of the equivalent-elliptic-cone prediction to typical flight conditions shows the pressure ratio decreases slightly. The extrapolation agrees more closely with Newtonian theory because at flight speeds and altitudes the curvatures of the body and shock are in closer alignment.

Centerline heating rates for various angles of attack are also plotted in Fig. 6 for Reynolds numbers between 1×10^6 and 4×10^6. The data are believed to be laminar, except at $\alpha = 53°$, where the last station showed a consistent increase in heating with increase in Reynolds number which is typical when transition to turbulent flow occurs. The solid lines are laminar heating predictions from a finite difference boundary-layer computer program[10] modified to account for streamline divergence as noted previously. The local flow conditions at the boundary-layer edge were assumed to be those on a cylinder inclined to the flow at an angle equivalent to the local body angle of attack. Near the nose the heating was underpredicted because the program was started by assuming the flow over the nose was that over a sharp cone. Beyond $x/L = 0.1$ the predicted values agree reasonably with the data. (Strip theory, modified for divergence, gave essentially the same predictions beyond $x/L = 0.2$ since pressure gradient effects were small.) It is believed that better agreement can be achieved when forthcoming, exact, inviscid flow calculations are used to obtain the boundary-layer edge conditions and the streamline divergence. The dashed curves represent estimates based on modified swept cylinder theory, Eq. (2), and they agree very well with the data ahead of the wing. In the region of the wing this latter theory under-predicts the heating and it is not shown.

The windward heating rates on the wing at $\alpha = 30°$ for no elevon deflection and for three span locations are plotted in Fig. 7. The heating rates are highest over the leading edge of the wing. Beyond the 30% chord location the heating rates are at about the same magnitude as those on the fuselage. The effect of Reynolds number variation on the heating ratios is negligible, indicating that the flow was probably laminar. However, later it is shown that at the highest Reynolds number, 7.24×10^6, transition from laminar to turbulent flow occurred on the fuselage centerline. Therefore, at this angle of attack, transition does not occur uniformly across the windward surface. (Other data at higher angles of attack shows transition probably occurs uniformly across the windward surface.) Near the midspan, where the flow is nearly two dimensional, data are compared with the crossflow theory from Ref. 4 assuming isentropic expansion from a normal shock pressure to a Newtonian pressure near the leading edge and to measured pressures over the remainder of the wing. This theory underpredicts the heating at and ahead of the 20% chord location, but otherwise agrees with the data.

It is of interest now to show the effects of elevon deflection

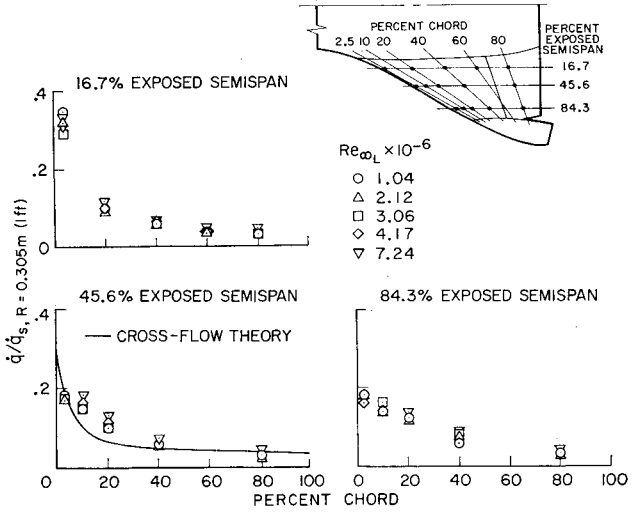

Fig. 7 Windward wing heating rates on NAR 134 delta-wing orbiter; $\alpha = 30°$.

on the flowfield and heating over the wing. Figure 8 is a sequence of photographs on the 129 delta-wing model at $\alpha = 15°$ showing the flow on the wing in the region of the elevon for three Reynolds numbers. The elevon is deflected 15° into the windward flow. At the low Reynolds number a separated region develops with reattachment along an oblique line across the elevon. Increasing the Reynolds number causes the extent of the separated region to diminish and regularly spaced vortices appear to be scrubbing the elevon surface; further increases in Reynolds number shows no separation and there appear to be vortices scrubbing the surface ahead and on the elevon. Thus, elevon aerodynamic control effectiveness will depend on Reynolds number.

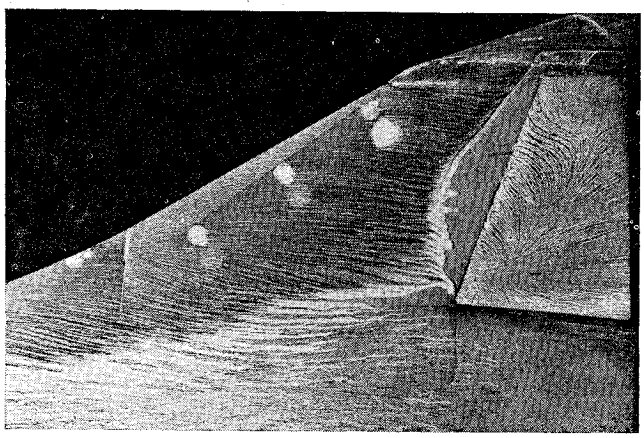

Fig. 8a Photographs of oil-flow patterns near deflected elevons; $L = 0.41$ m, and $\alpha = 15°$, $\delta_E = 15°$; $Re_{\infty L} = 1.4 \times 10^6$.

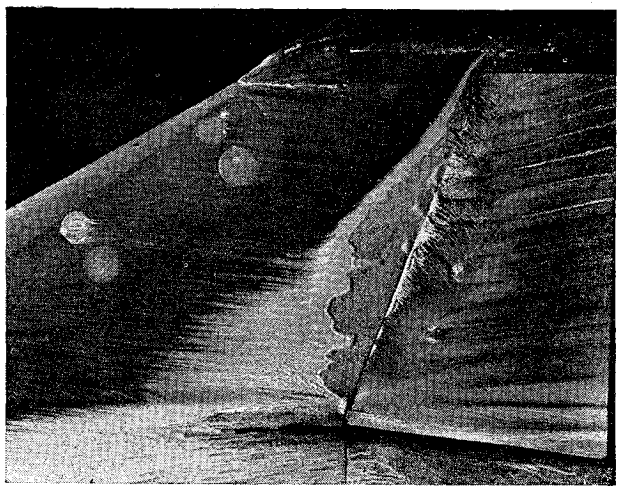

Fig. 8b Photographs of oil-flow patterns near deflected elevons; $L = 0.41$ m, and $\alpha = 15°$, $\delta_E = 15°$; $Re_L = 2.8 \times 10^6$.

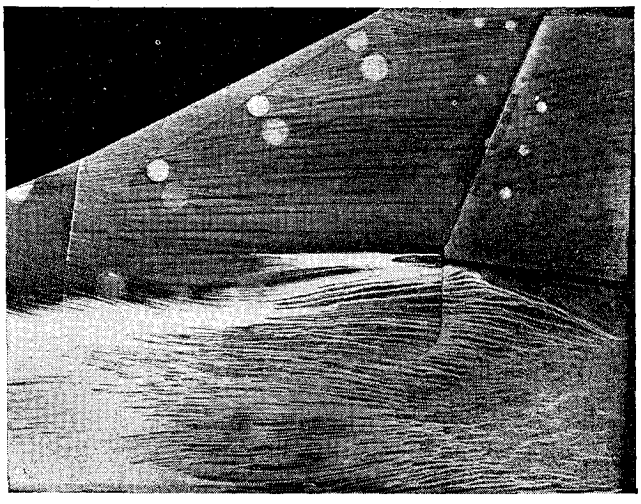

Fig. 8c Photograph of oil-flow patterns near deflected elevons; $L = 0.41$ m, and $\alpha = 15°$, $\delta_E = 15°$; $Re_{\infty L} = 5.7 \times 10^6$.

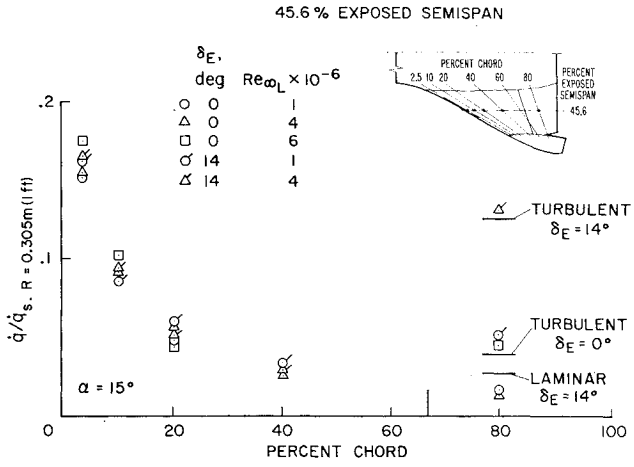

Fig. 9 Effect of elevon deflection on wing heating distribution; $\alpha = 15°$.

Corresponding windward wing heating rates measured on the 134 delta wing model are shown in Fig. 9. For no elevon deflection (unflagged symbols), the highest Reynolds number data suggest the flow is becoming turbulent ahead of the elevon, which explains why no separation region appeared on the oil flow patterns. Deflecting the elevons into the flow increases the heating on the elevon. The magnitude of the increase depends on the Reynolds number. The solid lines marked laminar and turbulent are estimates of the elevon heating rate for fully attached flows assuming wedge properties at the boundary-layer edge. The wedge angle was equal to the angle of inclination of the local surface relative to the free-stream direction. The low Reynolds number data for the deflected elevon lie above the attached laminar estimate because the separated boundary layer is probably reattaching near the measuring station. The higher Reynolds number data where vortices may be present indicate the deflected elevon heating can approach the estimated turbulent levels even though the undeflected elevon data are not turbulent. This undesirable heating problem can be eliminated by designing the vehicle to trim at an angle near that required to achieve maximum lift-to-drag ratio so that angle of attack may be modulated aerodynamically by elevon deflections away from the windward surface.

Turbulent heating rate data on the windward centerline of the delta wing orbiter are shown in Fig. 10. The data at $\alpha = 30°$ were obtained on the thin-walled model instrumented with thermocouples; the data at $\alpha = 10°$ were obtained on the model made of stycast and using the phase-change paint technique. The heating rates are laminar over the first half of the model. Transition to turbulent flow occurs rapidly and turbulent heating exists over the remaining 20–30% of the body length. The laminar rates compare favorably with predictions, accounting for divergence as shown previously. The turbulent rates also compare reasonably well with the trends predicted by the turbulent strip theory accounting for divergence as given by Eq. (6). As mentioned previously, corrections to strip theory accounting for divergence are small for turbulent flow. The origin of the turbulent flow was assumed to be at the onset of transition, and Reynolds analogy factor was taken to be 1.0

An example of the delta wing leeside centerline heating is shown in Fig. 11. Between the nose and canopy, where streamline oil flow patterns showed vortex-scrubbing on the

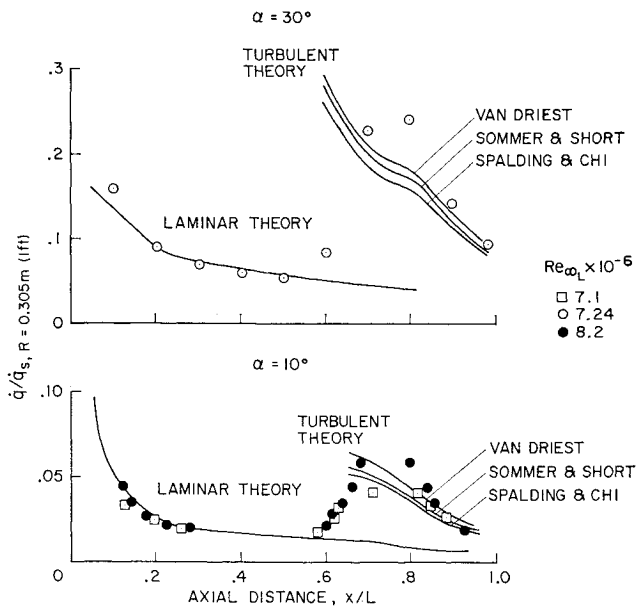

Fig. 10 Windward centerline turbulent heating rates on NAR delta-wing orbiters.

surface, the heating increases with increasing Reynolds number. At the canopy, where the vortex flow is impinging, the heating shows a marked increase. Beyond the canopy, where the flow is separated, the heating is lower and no substantial changes occur with increasing Reynolds number. The results described above are for a single Mach number, a parameter that will affect separation and vortex formation. Much more study is required before side and leeside temperatures can be estimated adequately for flight speeds and altitudes.

Transition Results

A formidable problem with defining the thermal environment encountered by space shuttle vehicles is transition from laminar to turbulent flow. Some heating distributions discussed previously showed the effects of transition on heating. Table 1 presents the locations of the beginning of transition obtained from various sets of windward centerline heating data taken in the Ames 3.5 tunnel. Only the data where a quantitative definition of transition could be made are shown. These data were obtained on smooth models, but the "dusty" test environment caused by the fine sediment from pebble erosion in the tunnel heater did create a certain amount of model pitting during the tests. The data shown as tripped were those where pitting may have been excessive. Later, some tests with controlled roughness will be discussed.

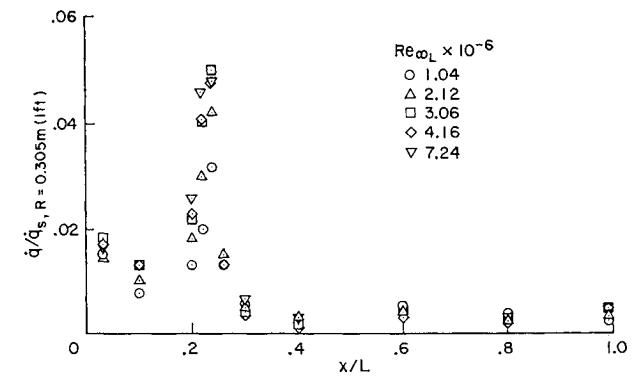

Fig. 11 Leeside centerline heating rates on the NAR-134 delta-wing orbiter; $L = 0.323$ m and $\alpha = 30°$.

In Fig. 12 these transition data are compared with two transition criteria proposed during the earlier phases of the space shuttle preliminary design.[20,21] The criteria were developed using data on cones and slender delta wings from wind-tunnel tests and some additional flight-test data. In preparing the comparisons, care was taken to evaluate local flow conditions and momentum thicknesses according to the methods employed by the original investigators. The present data on actual shuttle configurations generally lie above these criteria, indicating a conservative prediction for the wind-tunnel transition location. More test data on shuttle shapes for a wider range of Mach number and Reynolds number and a better understanding of the local boundary-layer edge conditions will be required before adequate correlations useful for extrapolating to flight speeds and altitudes are available.

An important aspect of the transition problem is the effect of roughness introduced by practical construction of a reusable, radiatively cooled surface. Therefore, some tests were performed to determine the effects of simulated heat shield panels on boundary-layer transition. The fuselage of the MSC straight-wing orbiter model was tested with simulated panels. The resulting heating distributions are compared in Fig. 13 with those obtained on a smooth model. The simulated panels on the full scale vehicle would by 0.625 m (2 ft) × 0.625 m (2 ft) with gaps 2.0 cm (0.8 in.) wide by

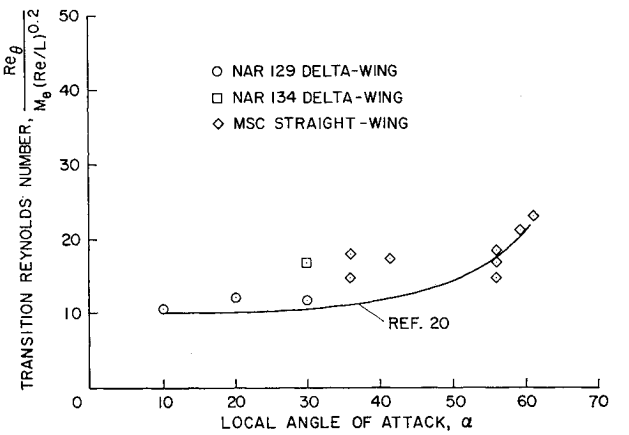

Fig. 12a Comparison of transition data with proposed criterion, transition Reynolds number based on momentum thickness vs angle of attack.

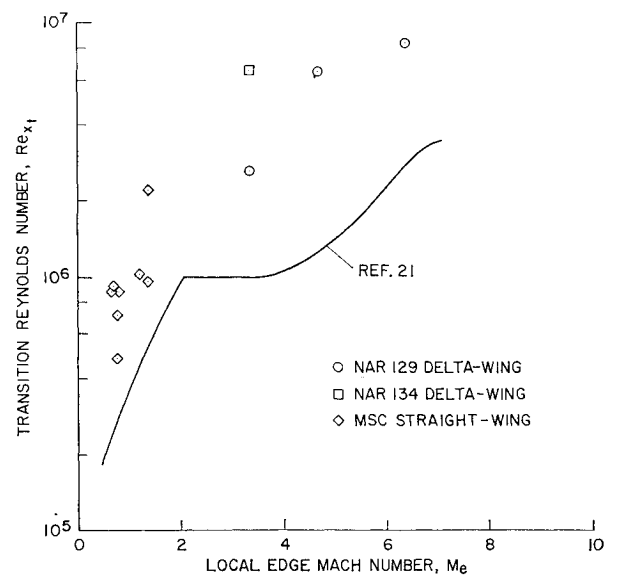

Fig. 12b Comparison of transition data with proposed criterion, transition Reynolds number vs local Mach no.

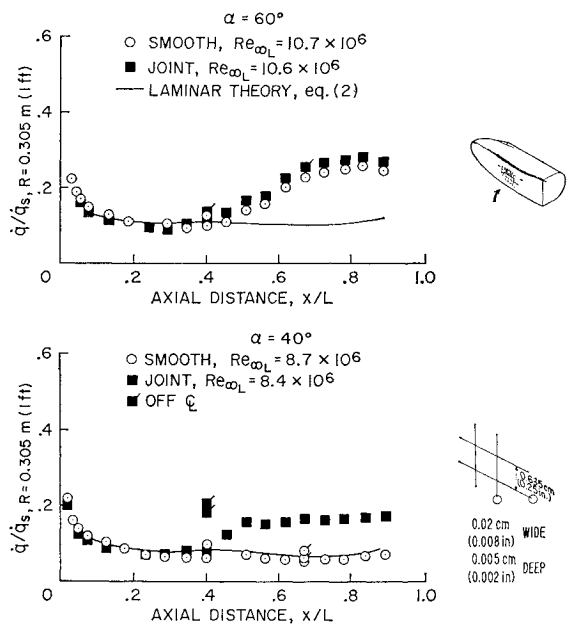

Fig. 13 Effect of simulated panel joints on boundary-layer transition on MSC straight-wing fuselage.

0.5 cm (0.2 in.) deep. At $\alpha = 60°$ the simulated panel joints had little effect on the location of transition, but at $\alpha = 40°$ they had a significant effect. The exact cause for the dramatic differences at the two angles of attack is still being studied, but changes in local cross flow, local Mach number, and boundary-layer thickness all probably have affected the results. Further, systematic tests to assess the influence of roughness on transition for the delta-wing are planned.

Conclusions

The foregoing examples of surface oil-flow patterns and heating distributions illustrate some of the problem areas involved in understanding the thermal environment encountered by typical shuttle vehicles. The flowfields over these vehicles are three-dimensional and complex. However, there are instances where realistic estimates of heating rates and pressures can be made, provided some account is taken of the three-dimensionality of the flow (e.g., along fuselage centerlines for laminar and turbulent flows). Such estimates not only help to interpret the test results but provide means for extrapolating test data to actual flight conditions.

Table 1 Transition locations; $M_\infty = 7.4$, $T_w/T_o = 0.4$

		p_o		T_o		
α	α_w	kn/m²	psia	°K	°R	$(x/L)_t$
MSC fuselage without wing (smooth model)						
60	56	2758	400	750	1350	0.71
60	56	4619	670	772	1390	0.66
60	56	6412	930	783	1410	0.60
60	60	8136	1180	772	1390	0.52
60	61.2	9928	1440	778	1400	0.44
40	36	6412	930	761	1370	0.57 (Tripped?)
40	36	8274	1200	761	1370	0.83
40	41.5	9928	1440	789	1420	0.4 (Tripped?)
40	36	11170	1620	767	1380	0.75
NAR 134 delta wing						
15	15	9928	1440	839	1510	0.56
15	15	10273	1490	772	1390	0.55
20	20	10273	1490	783	1410	0.52
30	30	10273	1490	783	1410	0.54
10[a]	10	10756	1560	772	1390	0.53
20[a]	20	10825	1570	833	1500	0.42
30[a]	30	8343	1210	827	1490	0.29 (Tripped?)

[a] Phase-change paint data and larger delta wing (NAR 129).

References

[1] Tischler, A. O., "Defining a Giant Step in Space Transportation," *Astronautics and Aeronautics*, Vol. 9, No. 2, Feb. 1971, pp. 22–25.

[2] Katzen, E. D., Marvin, J. G., Seegmiller, H. L., Axelson, J. J., Brownson, J. W., Lockman, W. K., and Kaattari, G. E., "Static Aerodynamics, Flow Fields and Aerodynamic Heating of Space Shuttle Orbiters," TM X-52876, Vol. I, July 1970, NASA, pp. 142–193.

[3] Marvin, J. G., Lockman, W. K. Mateer, G. G., Seegmiller, H. L., Pappas, C. C., DeRose, C. E., and Kaattari, G. E., "Flow Fields and Aerodynamic Heating of Space Shuttle Orbiters," TMX-2272, Vol. I, April 1971, NASA, pp. 21–73.

[4] Beckwith, I. E. and Cohen, N. B., "Application of Similar Solutions to Calculation of Laminar Heat Transfer on Bodies With Yaw and Large Pressure Gradient in High Speed Flow," TN D-625, 1961, NASA.

[5] Beckwith, I. E. and Gallager, J. J., "Local Heat Transfer and Recovery Temperatures on a Yawed Cylinder at a Mach Number of 4.15 and High Reynolds Numbers," TR R-104, 1961, NASA.

[6] Inouye, M., Marvin, J. G., and Sinclair, A. R., "Comparison of Experimental and Theoretical Shock Shapes and Pressure Distributions on Flat-Faced Cylinders at Mach 10.5," TN D-4397, 1968, NASA.

[7] Bertram, M. H. and Henderson, A., Jr., "Recent Hypersonic Studies of Wings and Bodies," *ARS Journal*, Vol. 31, No. 8, Aug. 1961, pp. 1129–1139.

[8] Vaglio-Laurin, R., "Laminar Heat Transfer on Three Dimensional Blunt Nosed Bodies in Hypersonic Flow," *ARS Journal*, Vol. 29, No. 2, Feb. 1959, pp. 123–129.

[9] Vaglio-Laurin, R., "Heat Transfer on Blunt Nosed Bodies in General Three-Dimensional Hypersonic Flow," Heat Transfer and Fluid Mechanics Institute, Univ. of California, Los Angeles, Calif., June 11–13, 1959.

[10] Marvin, J. G. and Sheaffer, Y. S., "A Method for Solving the Nonsimilar Laminar Boundary-Layer Equations Including Foreign Gas Injection," TN D-5516, 1969, NASA.

[11] Hayes, W. D., "Three Dimensional Boundary Layer," NAVORD Rep. 1313 (NOTS 384), May 1951, work supported by Bureau of Ordnance Task Assignment NOTS-36-Re 34-441-3. US Naval Ordinance Test Station, Inyokern, China Lake, Calif.

[12] Holdaway, G. H., Polek, T. E., and Kemp, J. H., Jr., "Aerodynamic Characteristics of a Blunt Half-Cone Entry Configuration at Mach Numbers of 5.2, 7.4, 10.4," TM X-782, 1963, NASA.

[13] Polek, T. E., Holdaway, G. H., and Kemp, J. H., Jr., "Flow Field and Surface Pressures on a Blunt Half-Cone Entry Configuration at Mach Numbers of 7.4 and 10.4," TM X-1014, 1964, NASA.

[14] Faget, M. A., "Space Shuttle: A New Configuration," *Astronautics and Aeronautics*, Vol. 8, No. 1, Jan. 1970, pp. 52–61.

[15] Jones, R. A. and Hunt, J. L., "Use of Fusible Temperature Indicators for Obtaining Quantitative Aerodynamic Heat-Transfer Data," TR R-230, Feb. 1966, NASA.

[16] Fay, J. A. and Riddell, F. R., "Stagnation Point Heat Transfer in Dissociated Air," *Journal of the Aerospace Sciences*, Vol. 25, No. 2, 1958, pp. 73–85.

[17] Seegmiller, H. L., "Shock Interference and Density Ratio Effects. Part I, Flow Field Visualization, Thermocouple Measurements, and Analysis," TMX-2272, Vol. I, April 1971, NASA, pp. 185–215.

[18] Hopkins, E. J., Rubesin, M. W., Inouye, M. Kerner, E. R., Mateer, G. G., and Polek, T. E., "Summary and Correlation of Skin Friction and Heat Transfer Data for a Hypersonic Turbulent Boundary Layer on Simple Shapes," TN D-5089, 1969, NASA.

[19] Kaattari, George G., "Estimation of Shock Layer Thickness and Pressure Distribution on Conical Bodies," TM X-62,031, 1971, NASA.

[20] Masek, R. V., "Boundary Layer Transition on Lifting Entry Vehicle Configurations at High Angle-of-Attack," TM X-52876, Vol. 1, 1970, NASA, pp. 445–462.

[21] Moote, J. D., "A Minimum Heating Flight Mode for High Lateral Range Space Shuttle Entries Including the Effects of Transition" TM X-52876 Vol. I 1970 NASA, pp. 531–546.